Size-dependent regulation of synchronized activity in living neuronal networks

Hideaki Yamamoto, Shigeru Kubota, Yudai Chida, Mayu Morita, Satoshi Moriya, Hisanao Akima, Shigeo Sato, Ayumi Hirano-Iwata, Takashi Tanii, and Michio Niwano

Phys. Rev. E **94**, 012407 — Published 13 July 2016

DOI: 10.1103/PhysRevE.94.012407

Size-dependent regulation of synchronized activity in living neuronal networks

Hideaki Yamamoto,[1,*] Shigeru Kubota,[2] Yudai Chida,[3] Mayu Morita,[4] Satoshi Moriya,[3] Hisanao Akima,[3] Shigeo Sato,[3] Ayumi Hirano-Iwata,[5] Takashi Tanii,[4] and Michio Niwano[3]

[1] *Frontier Research Institute for Interdisciplinary Sciences, Tohoku University, Sendai 980-8578, Japan*

[2] *Graduate School of Science and Engineering, Yamagata University, Yamagata 992-8510, Japan*

[3] *Research Institute for Electrical Communication, Tohoku University, Sendai 980-8577, Japan*

[4] *School of Fundamental Science and Engineering, Waseda University, Tokyo 169-8555, Japan*

[5] *Graduate School of Biomedical Engineering, Tohoku University 980-8579, Sendai, Japan*

* h-yamamoto@bme.tohoku.ac.jp

Abstract

We study the effect of network size on synchronized activity in living neuronal networks. Dissociated cortical neurons form synaptic connections in culture and generate synchronized spontaneous activity by 10 days *in vitro*. Using micropatterned surfaces to extrinsically control the size of neuronal networks, we show that synchronized activity can emerge in a network as small as 12 cells. Furthermore, a detailed comparison of *small* (~20 cells), *medium* (~100 cells), and *large* (~400 cells) networks reveal that synchronized activity become destabilized in the *small* networks. A computational modelling of neural activity is then employed to explore the underlying mechanism responsible for the size effect. We find that the generation and maintenance of the synchronized activity can be minimally described by (1) the stochastic firing of each neuron in the network, (2) enhancement in the network activity in a positive feedback loop of excitatory synapses, and (3) Ca-dependent suppression of bursting activity. The model further shows that the decrease in total synaptic input to a neuron that drives the positive feedback amplification of correlated activity is a key factor underlying the destabilization of synchrony in smaller networks. Spontaneous neural activity plays a critical role in cortical information processing, and our work constructively clarifies an aspect of the structural basis behind this.

I. INTRODUCTION

Temporal regulation of coherent neuronal activity is critical for the development and functioning of the brain [1,2]. The mammalian brain is a complex network of interacting subsystems, which consist of several tens to hundreds of neurons [3,4]. Although the dynamics in complex networks is strongly affected by the number of its constituent nodes [5,6], its effect on coherent activity is nontrivial, since multiple parameters such as network topology, node degrees, and coupling strengths also influence the dynamics. Because of this, a defined experimental system to determine how synchronous activity is generated and regulated in living neuronal networks of finite sizes is needed.

A network of cultured neurons provides a simple yet irreplaceable model system for studying the dynamics of neuronal systems. After several days of culture, neurons form synaptic contacts and the network begins to spontaneously generate bursting activity that propagates across the whole network within several tens to a hundred of milliseconds, which we refer to as the "synchronized" activity [7-18]. This activity is a network phenomenon, triggered by cooperation of the local noise dynamics and anatomical connectivity [17]. One of the major significance of cultured neurons in neurodynamics research is their controllability. For instance, using a micropatterned surface as a scaffold for culturing neurons, it is possible to extrinsically control the number of neurons comprising each network and the area they occupy [19-21]. This enables us to constructively study how network size affects synchrony in a living neuronal system.

In the current work, we investigate the mechanism underlying the emergence of synchrony in a network of neurons. We focus especially on the effect of network size in determining the level of synchrony while maintaining the other parameters, such as network topology, cell density, and culture duration constant. Neuronal activity is measured using

fluorescence Ca imaging, and the results are compared with computational simulations of spiking neural networks with a similar number of network nodes.

II. MATERIALS AND METHODS

A. Mircopatterned cortical networks

Electron-beam (EB) lithography was used to fabricate micropatterns on coverslips for cell patterning. Poly-D-lysine (PDL) and 2-[methoxy(polyethyleneoxy)propyl]trimethoxysilane (mPEG) were used as cell-permissive and non-permissive coatings, respectively [22,23]. Briefly, glass coverslips (diameter, 15 mm; thickness, 0.17 mm; Warner Instruments CS-15R15) were cleaned in piranha solution and modified with mPEG. An EB resist was then spin-coated on the surface, and EB lithography was performed. The pattern was transferred to the mPEG layer by O_2 plasma ashing, and the exposed area was then modified with PDL. The sample was finally sonicated in tetrahydrofuran and ethanol to remove the EB resist and the unbound PDL. The coverslips were then sealed onto the bottom of a 35-mm plastic dish with a 12-mm hole, using a paraffin/petrolatum (3:1) mixture [24].

Primary neurons were obtained from rat cortices at embryonic day 18. Neurons were plated on the micropatterned coverslips and cocultured with astrocyte feeder cells in N2 medium (Minimal Essential Medium + N2 supplement + 0.5 mg ml^{-1} ovalbumin + 10 mM HEPES) [22,24,25]. After 5 days, cytosine arabinoside was added to a final concentration of 1 μM to stop the proliferation of contaminating glial cells. The cells were maintained in culture for 10 days before neural activity was measured.

Fluorescence Ca imaging was used to evaluate spontaneous neuronal activity of the micropatterned neuronal networks. The cells were first rinsed in HEPES-buffered saline (HBS) containing (in mM): 128 NaCl, 4 KCl, 1 $CaCl_2$, 1 $MgCl_2$, 10 D-glucose, 10 HEPES, and 45

sucrose. Then the cells incubated at 37°C in HBS containing 2 μM Fluo-4 AM and 0.01% Pluronic F-127. After 30 min, the cells were rinsed with HBS and incubated for an additional 10 min to complete the de-esterification of the loaded dyes. Imaging was conducted on an inverted microscope (Nikon Eclipse TE300) equipped with 20× objective lens (NA, 0.75), 100 W mercury arc lamp, fluorescence filter (EX 470/20, DM 500, BA 515), and a cooled-CCD camera (Hamamatsu Orca-ER). All recordings were made at room temperature. Images were collected at 5 Hz on HCImage software (Hamamatsu).

The image sequences were analyzed off-line with the ImageJ (NIH) and custom-written Perl program. To detect neural activity of each cell, a circular region of interest was manually set around the soma of the cell, and the change in relative fluorescence intensity $\Delta F/F$ was calculated from raw fluorescence intensity F using a previously reported algorithm [26]. A time derivative of $\Delta F/F$ was then calculated and was thresholded at 2.58×SD of noises to mark the onset of burst firing [27]. This procedure was necessary in order to extract the rising phase of the Ca signals, which corresponds to the timing of burst neural firing. The SD of the noise was determined from 10 cells recorded in the presence of a Na-channel blocker, tetrodotoxin (1 μM). Sporadic action potentials were neglected in the analysis. The termination of the bursting activity was determined from the time point where the derivative returned back to zero.

B. Spiking neural network models

The network model consisted of N leaky integrate-and-fire neurons, with the value for N ranging from 20 to 2000. All neurons were excitatory and were connected randomly [15,16] with an average node degree of k. GABA, the principal inhibitory neurotransmitter in the cortex, acts as an excitatory neurotransmitter in young cultures and transiently acquires its inhibitory action

starting at around 6 DIV [14,17,18,28,29]. This reversal of GABA function is known as the GABA switch and completes by 18 DIV [14,28]. Since the culture used in this work was at the early stage of the GABA switch, we constructed our computational network solely with excitatory neurons to simplify the model.

A total of at least 50 networks were sampled for each N, and we denote the average k of the sampled networks as $\langle k \rangle$. Considering that an axon of a neuron grows longer than a side of a micropattern L, the number of target neurons that a neuron synapses on can also be expected to increase proportionally with L. This implies that $\langle k \rangle$ may be proportional to $\sqrt{N}$, since N is nearly proportional to the micropattern area L^2 in networks with a constant cell density [see Fig. 1(d)]. Therefore we simply assumed the average node degree to be $\langle k \rangle = \sqrt{N}$. We further considered culture-to-culture variations in the density of synaptic connections by distributing k normally around $\langle k \rangle$ with a SD of $0.3 \times \langle k \rangle$. Networks that exhibit bursts with physiologically implausible durations were occasionally sampled for $N > 1000$. We excluded the sample from the statistics when there was more than one burst with a duration of over 10 s.

Major parameters used in the simulation were taken from previous reports, and their values are physiological [30-32]. The membrane potential of a neuron i at time t, $V_i(t)$, was calculated by

$$\tau_{\mathrm{mem}} \frac{\mathrm{d}V_i(t)}{\mathrm{d}t} = E_{\mathrm{L}} - V_i(t) + R_{\mathrm{in}}\, I_{\mathrm{tot}}(t)$$

where τ_{mem} = 20 ms is the membrane time constant, E_{L} = -74 mV the resting potential, R_{in} = 40 MΩ the input resistance, and $I_{\mathrm{tot}}(t)$ the input current [30]. The time step dt was 0.1 ms, and each calculation was carried out for 200 s. When $V_i(t)$ exceeded the threshold value of V_{th} = -54 mV, an action potential was generated and the membrane potential was reset to V_{reset} = -60 mV [30]. After an action potential, the membrane potential was held constant at V_{reset} for 1 ms, which reflects the absolute refractory period.

The total input current $I_{\mathrm{tot}}(t)$ was calculated based on the model described by French and Gruenstein [31]:

$$I_{\mathrm{tot}}(t) = \sum_j I_j(t) + I_{\mathrm{K(Ca)}}(t) + I_{\mathrm{ref}}(t) + \xi(t)$$

where $I_j(t)$ is the synaptic input from neuron j, $I_{\mathrm{K(Ca)}}(t)$ the Ca-dependent K current, $I_{\mathrm{ref}}(t)$ the refractory current, and $\xi(t)$ the noise. The synaptic current was calculated by

$$I_j(t) = g_{\mathrm{syn}}(t)\left[E_{\mathrm{syn}} - V(t)\right]$$

$$g_{\mathrm{syn}}(t) = \sum_k A_{\mathrm{syn}}\left[\exp\left(-\frac{t-t_{j,k}}{\tau_{\mathrm{syn1}}}\right) - \exp\left(-\frac{t-t_{j,k}}{\tau_{\mathrm{syn2}}}\right)\right]$$

where $g_{\mathrm{syn}}(t)$ is the synapse conductance at time t, E_{syn} = 0 mV the synaptic reversal potential, A_{syn} = 5 nS the maximal synapse conductance, τ_{syn1} = 5.3 ms and τ_{syn2} = 0.2 ms are the synaptic time constants, and $t_{j,k}$ is the time of kth firing of neuron j. The function and time constants were taken from Ref. 32, and the synapse conductance was adjusted to resemble the model for cultured neurons in Ref. 31.

The current $I_{\mathrm{K(Ca)}}(t)$ was given by

$$I_{\mathrm{K(Ca)}}(t) = g_{\mathrm{K(Ca)}}c(t)[E_{\mathrm{K}} - V(t)]$$

$$\frac{\mathrm{d}c(t)}{\mathrm{d}t} = c_{\mathrm{Step}}\sum_k \delta(t-t_k) - \frac{c(t)}{\tau_{\mathrm{Ca}}}$$

where $g_{\mathrm{K(Ca)}}$ = 10.0 nS $\mu\mathrm{M}^{-1}$ is the Ca-dependent K conductance, $c(t)$ the intracellular Ca concentration, E_{K} = -75 mV the reversal potential of the K current, c_{Step} = 0.1 μM the step influx of Ca triggered by an action potential, t_k the time of kth action potential, and τ_{Ca} = 2700 ms the time constant of Ca dynamics.

The third term $I_{\mathrm{ref}}(t)$ is the refractory current calculated by

$$I_{\mathrm{ref}}(t) = -g_{\mathrm{ref}}\left(1 + \frac{t-t_k}{\tau_{\mathrm{ref}}}\right)^{-1} P_{\mathrm{ref}}(t-t_k)(V(t) - V_{\mathrm{reset}})$$

147

$$P_{\text{ref}}(t - t_k) = \begin{cases} 1 & \text{for } t_k < t < t_{k+1} \\ 0 & \text{otherwise} \end{cases}$$

148 with g_{ref} = 150 nS and τ_{ref} = 12 ms. This term suppresses burst firing at supra-physiological
149 frequencies.

150 The fourth term is the noise current given by

$$\xi(t) = M_N \sum_k \alpha\left(t - t_k^N; r_N; \tau_N\right)$$

151

$$\alpha(s; r; \tau) = \frac{\mathrm{e}^{-s/\tau} - \mathrm{e}^{-s/r}}{\mathrm{e}^{-\bar{s}/\tau} - \mathrm{e}^{-\bar{s}/r}} \quad \text{with} \quad \bar{s} = \frac{r\tau \ln(r/\tau)}{r - \tau}$$

152 where M_{N} = 1000 pA is the amplitude of the noise, t_k^{N} the onset of the kth noise event, r_{N} = 30
153 ms, and τ_{N} = 50 ms. The event was generated by a stationary Poisson process (0.5 Hz). The
154 rather high value of M_{N} was used to allow neurons to be reactivated after an occurrence of a
155 network burst that raises the inhibitory current $I_{\text{K(Ca)}}$.

156

157 ## III. RESULTS

158 ### A. Size-dependent dynamics of micropatterned cortical networks

159 We first investigated the spatiotemporal patterns of spontaneous activity in neuronal networks of
160 three different sizes: 200×200 μm^2 (*small*; n = 19 networks), 500×500 μm^2 (*medium*; n = 17
161 networks), and 1000×1000 μm^2 (*large*; n = 19 networks). As shown in the phase-contrast
162 micrographs, neurons grew selectively inside the micropattern with well-spread cell bodies,
163 thick dendrites, and a uniformly growing axon meshwork [Fig. 1(a-c)]. The average number of
164 cells in the networks was 23, 124, and 445 for the *small*, *medium*, and *large* networks,
165 respectively, giving a nearly constant cell density among the three patterns [Fig. 1(d)].

166 Figs. 2(a-c) show micropatterned neuronal networks loaded with a fluorescence Ca

167 indicator Fluo-4. Measurements of spontaneous neural activity revealed that all three of the
168 networks generate globally synchronized network bursts. Synchronized activity appeared even
169 in a *small* network that consisted of only 12 cells [Fig. 2(a)].

170 Fig. 3(a) shows fluorescence signals from 5 representative cells in a *large* network.
171 Raster plots of neural activity were obtained from the first derivative of the fluorescence signals
172 [Fig. 3(b)]. To evaluate the synchronized activity of the network, we defined "network bursts" as
173 neural activity that involves > 25% of the cells and that persisted for > 1 s. In the case of the
174 representative network shown in Fig. 3(b), network bursts were detected 6 times during a
175 imaging session of 360 s (16.7×10^{-3} Hz). The duration of each network burst was typically
176 between 2 and 3 seconds, as shown in a close-up view of the raster plot [Fig. 3(c)]. A
177 comparison of micropatterned networks of three different sizes revealed that the mean
178 frequencies of the network bursts were statistically insignificant in the case of *medium* and *large*
179 networks, while the frequency was significantly reduced in the *small* network [Fig. 3(d); $p <$
180 0.01].

181 Another prominent effect of size reduction was the appearance of asynchronous
182 activity in the small networks [Fig. 4(a)]. Such activity was observed both in networks that
183 generated network bursts (n = 11 of 19) and those that did not. To quantify the degree of
184 synchronization, we analyzed the correlation of neural activity in individual cells by evaluating
185 the correlation coefficient for neuronal pairs *i*-*j*, r_{ij}, as:

$$r_{ij} = \frac{\sum_t (f_i(t) - \overline{f_i})(f_j(t) - \overline{f_j})}{\sqrt{\sum_t (f_i(t) - \overline{f_i})^2}\sqrt{\sum_t (f_j(t) - \overline{f_j})^2}}$$

186

187 where $f_i(t)$ is the relative fluorescence intensity of cell i at time t, and $\overline{f_i}$ the time averaged
188 intensity. In *large* and *medium* networks, r_{ij} was nearly equal to 1 for the majority of the cell
189 pairs, indicating that the activity was highly synchronized among the entire population. In

contrast, networks that presented relatively low intercellular correlations were occasionally observed in the *small* networks [Fig. 4(b)]. A comparison of multiple networks revealed that the average correlation coefficient was significantly lower in the *small* network compared to the others [Fig. 4(c); $p < 0.01$]. In summary, a reduction in the network size in living neuronal networks decreased the frequency of synchronized network bursts and desynchronized neural activity. This effect was prominent in networks with $N < 100$ cells, for 10 DIV cortical networks with a nearly constant cell density.

B. Computational modelling of the size effect

We next investigated the cellular mechanism behind this size effect using computational models of neuronal networks consisting of N excitatory neurons (N = 20~2000) [Figs. 5(a) and 5(b)]. All parameters for the simulation were derived from previous reports and are physiologically validated [30-32]. Figs. 5(c) and 5(d) show representative raster plots of networks consisting of 20 and 400 neurons, respectively. Three characteristic traits could be observed that were in good agreement with the experimental observations: (1) rhythmic, synchronized firing patterns (network bursts) with a period of > 10 s [Fig. 5(d)], (2) decrease in the frequency of network bursts with decreasing network size, and (3) decrease in neuronal correlation with decreasing network size [Fig. 5(c)]. In the current model, the network bursts are triggered by the stochastic overlap of noise input, while its cessation is governed by the activity-dependent rise in intracellular Ca concentration and the resulting inhibitory K(Ca)-current. When the network size decreases, neurons have less chance of simultaneously receiving multiple noise inputs, and this decreased the occurrence of network bursts.

The decrease in neuronal correlation in smaller networks was confirmed in the computational models, which were quantitatively in agreement with the experimental results.

The dependence of the average correlation coefficient on network size is shown in Fig. 6. As a general trend, the average correlation coefficient decreased with network size. In a closer examination, it was found that the average correlation coefficient decreased gradually with the network size until $N \approx 100$ and then decreased rapidly in networks of $N < 100$. The calculated values were in good agreement with the experimental data both in the *N*-dependency and the absolute values.

Fig. 7 shows the dependence of the network burst frequency on network size. The frequency of network bursts was found to increase with network size, and the values agreed quantitatively well with the experimental data. One exception was the data for the *large* network, were the model gave a nearly two-fold higher frequency of network bursts. This is most likely due to the suppression of the growth of node degree in actual neuronal networks of larger sizes. Indeed, lowering $\langle k \rangle$ from 20 to 17 in a 400-neuron network decreased the frequency from 37.8×10^{-3} Hz to 20.2×10^{-3} Hz, the latter of which is close to the experimental value for the *large* network.

IV. DISCUSSION

The findings reported herein show that the globally synchronized activity of a cultured cortical network is altered when the network is composed of less than ~100 cells. The computational modelling based on physiologically derived parameters suggest that the major factor that caused the dynamics to change in $N < 100$ networks is the decrease in the number of synaptic inputs per neuron, although other factors, such as the number of noise or the level of noise, can also influence the degree of synchrony. In the current simulation, the firing of a presynaptic neuron depolarizes the postsynaptic neuron by ~2 mV. When networks are scaled and the number of inputs is 10 ($\langle k \rangle = 10$ corresponds to $N = 100$), the correlated firing of all presynaptic neurons

238 depolarizes a postsynaptic neuron by > 20 mV, which is sufficient to raise its membrane
239 potential above its threshold from its resting potential (V_{th} = -54 mV and V_{rest} = -74 mV) and
240 trigger an action potential. When the network size is smaller, the number of synaptic inputs
241 decreases. This means that such correlated activity fails to propagate, thus decreasing the chance
242 of network bursts to occur. We note that local network connectivity has also been shown to be
243 critical for the spontaneous generation of network bursts, in addition to the noise [17].
244 Previous works have shown that the connectivity in neuronal networks is affected by
245 experimental conditions such as cell density [12,13,29] or culture duration [7,29,35], both of
246 which correlate positively with neuronal activity. In the current experiment, we kept cell density
247 and culture duration constant (Fig. 1), and explored the effect of network size. Therefore, we
248 simply assumed in the model that the connectivity (average node degree) increases with the
249 network size as $\langle k \rangle = \sqrt{N}$.
250 According to Soriano *et al.*, the average node degree is approximately 100 for an
251 unpatterned cortical network of $N \approx 6.5\times10^4$ cells (500 neurons mm^{-2} on a 13-mm coverslip;
252 14-21 DIV) [29]. For a network of this size, a simple extrapolation of the square-root
253 relationship gives $\langle k \rangle \approx 250$; this is over two times the literature value. This mismatch could be
254 caused by the difference in the culture duration and by the inappropriateness of assuming the
255 square-root growth of $\langle k \rangle$ in very large networks. Axons continue their growth even after 10
256 DIV [10], during which the number of synapses [7,35] and connectivity [29] increase. The
257 deviation from the square-root dependence in larger cultures is a reasonable consequence of the
258 finite lengths of axons and dendrites that are shorter than the coverslip diameter [10]. Indeed,
259 saturation of the experimentally observed burst frequency in the *large*, 1×1 mm^2 networks [Figs.
260 3(d) and 7] supports the idea that the square-root dependence is applicable mainly in small-sized
261 networks.

From the perspective of information theory, an asynchronous state has a larger capacity for representing information in a population coding network [36]. Indeed, the spontaneous activity of *in vivo* cortical networks (rat visual cortex) is less correlated with an average correlation coefficient of ~0.1 [37,38]. The findings presented in this work enables us to consider the qualitative difference in the spatiotemporal pattern of spontaneous neural activity of *in vivo* and *in vitro* neuronal networks with regards to the size of the neuronal ensembles. Neurons of *in vitro* networks extend axons to a wide area and form strong synapses on a large number of neurons in that area. Contrarily, in networks *in vivo*, axons are guided by extracellular cues, synapses undergo activity-dependent pruning during development, and the resulting neuronal connections are highly structured. Our data imply that the *in vivo* networks are comprised of densely-connected neuronal modules with weak inter-module connections. This implication is in agreement with recent brain network analyses, which revealed the dominance of a modular network structure in the brain [4]. Moreover, it directs us to a future work that realistic models of *in vivo* networks can be fabricated *in vitro* using living neurons, by creating modular micropatterns. Consecutive recordings in longer imaging sessions, e.g., ~30 min [17], enable richer analysis of the activity statistics and would be important for studying such networks.

It is interesting to note that synchronization in neurons is qualitatively different from that of cardiomyocytes, in which synchrony occurs with only two cells. A cardiomyocyte is another type of cell with an excitatory membrane, and previous work using a microfabricated device has shown that the coupling of two cardiomyocytes is sufficient to generate synchronized beating [39]. In cardiomyocytes, inter-cellular coupling is mediated by gap junctions. The observation that a two-cell ensemble is sufficient to generate synchronized activity indicates that the firing of a single neighboring cell is sufficient to increase the membrane potential above the

threshold and to trigger an action potential in a cardiomyocyte. Contrarily, neuronal signal transmission is mainly mediated by chemical synapses. In central excitatory chemical synapses, the postsynaptic potential induced by a single cell is usually in the order of a tenth to a few mV [40], which is not sufficient to increase the membrane potential above the threshold and to trigger a neuronal action potential. Therefore multiple, simultaneous inputs are required to generate an action potential in a neuron, as previously described as the quorum firing [17,29,33,34]. This requirement of multiple inputs enables both the synchronous and asynchronous states to be present in neural systems, and we showed this in networks of different sizes. A similar phenomenon has been demonstrated in developing networks as well [29].

V. CONCLUSIONS

We reported on a constructive investigation of how the degree of spontaneous synchronized activity depends on the network size. Micropatterned substrates were used to restrict the size of cultured cortical networks. Spontaneous activity in *large* networks (~400 cells) was highly synchronized, resembling the activity observed in unpatterned networks. Both the frequency of synchronized firing and the intercellular correlation of neural activity decreased with network size, and, for networks comprised of ~20 cells, the average correlation coefficient decreased to <0.4. Using a computational model of spiking neuron networks, we further showed that the size effect can be explained through the following three mechanisms: (1) Poisson firing of individual neurons, (2) positive-feedback amplification of the activity through excitatory synaptic transmission, and (3) the Ca-dependent inhibition of generated bursts. Recent advancements in cortical physiology have revealed the active roles of spontaneous activity, such as encoding predictive information [41]. The effect of network scaling on synchronized bursting events has been considered in earlier studies, which studied its effect on the frequency of synchronized

bursting and the distribution of inter-burst intervals [19,21]. This work, to our knowledge, is the first to show the transition from synchronous to asynchronous firing in a size-dependent manner. Our findings provide a novel structural background regarding how the spatiotemporal pattern of spontaneous activity is generated in the brain.

ACKNOWLEDGEMENTS

The authors wish to thank Prof. Shun Nakamura (Tokyo University of Agriculture and Technology) for fruitful suggestions, and Mr. Sho Kono, Mr. Koji Ishihara, and Mr. Soya Fujimori (Waseda University) and Mr. Ryosuke Matsumura (Tohoku University) for technical assistance. This study was supported by the Cooperative Research Project Program of the Research Institute of Electrical Communication at Tohoku University, JSPS KAKENHI No. 15K17449 and 26390035, JST CREST Program, and a research grant from the Asahi Glass Foundation. R. M. was also supported by JSPS Research Fellowships for Young Scientists (15J03545).

References

[1] K. Benchenane, P. H. Tiesinga, and F. P. Battaglia, Curr. Opin. Neurobiol. **21**, 475 (2011).

[2] D. Senkowski, T. R. Schneider, J.J. Foxe, A.K. Engel, Trends Neurosci. **31**, 401 (2008).

[3] E. G. Jones, Proc. Natl. Acad. Sci. U. S. A. **97**, 5019 (2000).

[4] D. Meunier, R. Lambiotte, and E.T. Bullmore, Front. Neurosci. **4**, 200 (2010).

[5] A. Arenas, A. Díaz-Guilera, J. Kurths, Y. Moreno, and C. Zhou, Phys. Rep. **469**, 93 (2008).

[6] J. Aguirre, R. Sevilla-Escoboza, R. Gutiérrez, D. Papo, and J. M. Buldú, Phys. Rev. Lett. **112**, 248701 (2014).

[7] K. Muramoto, M. Ichikawa, M. Kawahara, K. Kobayashi, and Y. Kuroda, Neurosci. Lett. **163**, 163 (1993).

[8] R. Segev, Y. Shapira, M. Benveniste, and E. Ben-Jacob, Phys. Rev. E **64**, 011920 (2001).

[9] T. Tateno, A. Kawana, and Y. Jimbo, Phys. Rev. E **65**, 051924 (2002).

[10] T. Voigt, T. Opitz, and A. D. de Lima, J. Neurosci. **25**, 4605 (2005).

[11] D. A. Wagenaar, J. Pine, and S. M. Potter, BMC Neurosci. **7**, 11 (2006).

[12] M. Ivenshitz and M. Segal, J. Neurophysiol. **104**, 1052 (2010).

[13] D. Ito, H. Tamate, M. Nagayama, T. Uchida, S. N. Kudoh, and K. Gohara, Neuroscience **171**, 50 (2010).

[14] T. Baltz, A. D. de Lima, and T. Voigt, Front. Cell. Neurosci. **4**, 15 (2010).

[15] T. Baltz, A. Herzog, and T. Voigt, J. Neurophysiol. **106**, 1500 (2011).

[16] T. Gritsun, J. le Feber, J. Stegenga, and W. L. C. Rutten, Biol. Cybern. **105**, 197 (2011).

[17] J. G. Orlandi, J. Soriano, E. Alvarez-Lacalle, S. Teller, and J. Casademunt, Nat. Phys. **9**, 582 (2013).

[18] E. Tibau, M. Valencia, and J. Soriano, Front. Neural Circuits **7**, 199 (2013).

[19] R. Segev, M. Benveniste, E. Hulata, N. Cohen, A. Palevski, E. Kapon, Y. Shapira, and E.

348 Ben-Jacob, Phys. Rev. Lett. **88**, 118102 (2002).

349 [20] N. R. Wilson, M. T. Ty, D. E. Ingber, M. Sur, and G. Liu, J. Neurosci. **27**, 13581 (2007).

350 [21] M. Shein Idelson, E. Ben-Jacob, and Y. Hanein, PLoS ONE **5**, e14443 (2010).

351 [22] H. Yamamoto, T. Demura, M. Morita, G. A. Banker, T. Tanii, and S. Nakamura, J.

352 Neurochem. **123**, 904 (2012).

353 [23] H. Yamamoto, T. Demura, M. Morita, S. Kono, K. Sekine, T. Shinada, S. Nakamura, and T.

354 Tanii, Biofabrication **6**, 035021 (2014).

355 [24] K. Goslin and G. Banker, *Culturing Nerve Cells* (MIT Press, Cambridge, MA, 1991).

356 [25] S. Kaech and G. Banker, Nat. Prot. **1**, 2406 (2006).

357 [26] H. Jia, N. L. Rochefort, X. Chen, and A. Konnerth, Nat. Prot. **6**, 28 (2011).

358 [27] Y. Ikegaya, G. Aaron, R. Cossart, D. Aronov, I. Lampl, D. Ferster, and R. Yuste, Science

359 **304**, 559 (2004).

360 [28] K. Ganguly, A. F. Schinder, S. T. Wong, and M.-m. Poo, Cell **105**, 521 (2001).

361 [29] J. Soriano, M. Rodríguez Martínez, and E. Moses, Proc. Natl. Acad. Sci. U. S. A. **105**,

362 13758 (2008).

363 [30] T. W. Troyer and K. D. Miller, Neural Comput. **9**, 971 (1997).

364 [31] D. A. French and E. I. Gruenstein, J. Comput. Neurosci. **21**, 227 (2006).

365 [32] P. Dayan and L. F. Abbott, *Theoretical Neuroscience* (MIT Press, Cambridge, MA, 2001).

366 [33] I. Breskin, J. Soriano, E. Moses, and T. Tlusty, Phys. Rev. Lett. **97**, 188102 (2006).

367 [34] O. Cohen, A. Keselman, E. Moses, M. Rodríguez Martínez, J. Soriano, and T. Tlusty, EPL

368 **89**, 18008 (2010).

369 [35] G. J. Brewer, M. D. Boehler, R. A. Pearson, A. A. DeMaris, A. N. Ide, and B. C. Wheeler, J.

370 Neural Eng. **6**, 014001 (2009).

371 [36] S. Hanslmayr, T. Staudigl, and M.-C. Fellner, Front. Human Neurosci. **6**, 74 (2012).

372 [37] D. S. Greenberg, A. R. Houweling, and J. N. D. Kerr, Nat. Neurosci. **11**, 749 (2008).

373 [38] Y. H. Ch'ng and R. C. Reid, Front. Integ. Neurosci. **4**, 20 (2010).

374 [39] K. Kojima, T. Kaneko, and K. Yasuda, Biochem. Biophys. Res. Commun. **351**, 209 (2006).

375 [40] S. Song, P. J. Sjöstöm, M. Reigl, S. Nelson, and D. B. Chklovskii, PLoS Biol. **3**, e68
376 (2005).

377 [41] P. Berkes, G. Orbán, M. Lengyel, and J. Fiser, Science **331**, 83 (2011).

Figure captions

FIG. 1. Primary rat cortical neurons grown on micropatterned substrates at 10 DIV. The size of the micropatterns were: (a) 200×200 μm^2 (*small*), (b) 500×500 μm^2 (*medium*), and (c) 1000×1000 μm^2 (*large*). Scale bars, (a,b) 100 μm and (c) 200 μm. (d) The number of cells on each micropattern. Boxes indicate the span from the median to the first and third quartiles, whiskers the whole data spread, and circular plots the mean. The number of cells was determined from phase-contrast micrographs.

FIG. 2 (color online). Fluorescence Ca imaging of micropatterned neuronal networks. The cells were loaded with the fluorescence Ca indicator Fluo-4. (a) Time lapse images of a synchronized network burst observed in a 12-cell network on the *small* micropattern. (b,c) Cortical networks on (b) medium and (c) large micropatterns loaded with Fluo-4.

FIG. 3 (color online). Analysis of spontaneous neural activity in micropatterned cortical networks. (a) Relative fluorescence intensity of the Ca indicator Fluo-4 in a *large* network. Traces from 5 representative cells are shown. (b) Raster plot of the spontaneous neural activity for a *large* network derived from the relative fluorescence intensity. Each point corresponds to a bursting activity in a neuron, determined from the derivative of the fluorescence trace. In this particular example, synchronized network bursts were detected 6 times during a 360 s recording session. Note that a fraction of the neurons randomly selected from the whole population was analyzed. (c) A close-up view of a network burst. (d) Frequency of network bursts for the three network sizes. Boxes indicate the span from the median to the first and third quartiles, whiskers the whole data spread, and circular plots the mean.

FIG. 4 (color online). Effect of network size on synchrony. (a)Raster plot of the spontaneous neural activity for a *small* network. (b) Matrix plot of correlation coefficients of the network shown in (a). (c) Average correlation coefficient calculated for each network size. Boxes indicate the span from the median to the first and third quartiles, whiskers the whole data spread, and circular plots the mean.

FIG. 5 (color online). Computational simulation of spontaneous neural activity in cultured cortical networks of different sizes. (a,b) Schematic illustration of network models. Blue squares are the nodes (neurons), and gray lines are the links. (c,d) Raster plot derived from the model network. Number of neurons, N, and average node degree, k, were: (a,c) $N = 20$, $k = 4.5$ and (b,d) $N = 400$, $k = 20$.

FIG. 6 (color online). Dependence of average correlation coefficient on network size. The blue line represents the mean of the simulation data. For comparison, the experimental results are plotted in red. The simulation data over a wider range is shown in the inset.

FIG. 7 (color online). Dependence of the network burst frequency on network size. The blue line represents the mean of the simulation data. For comparison, the experimental results are plotted in red. The simulation data over a wider range is shown in the inset.

Figures

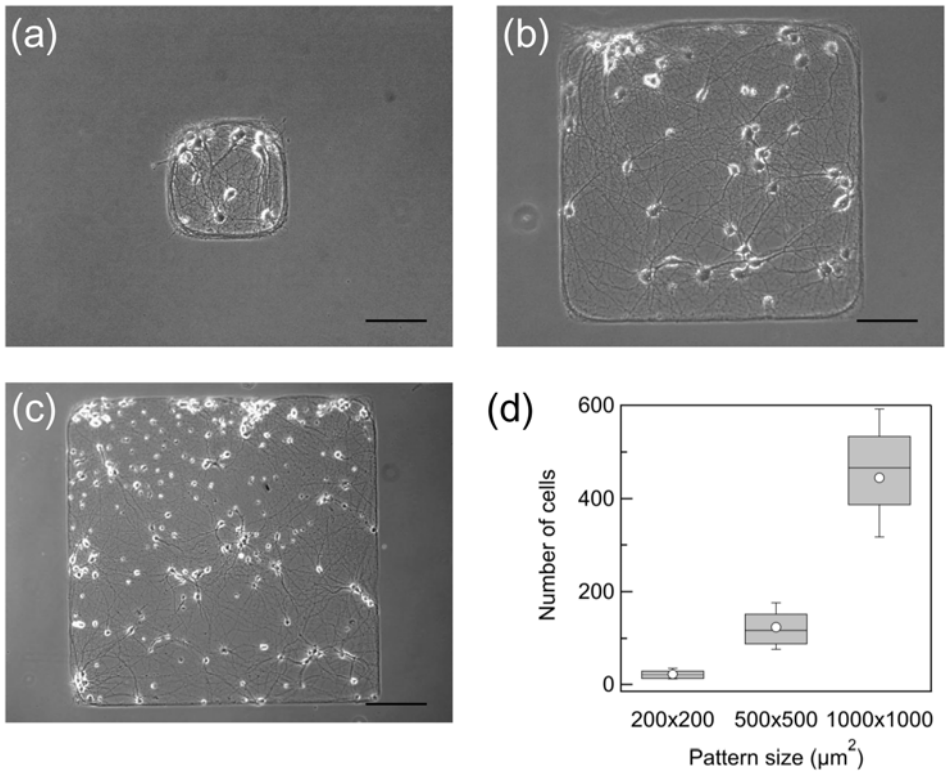

Figure 1

426

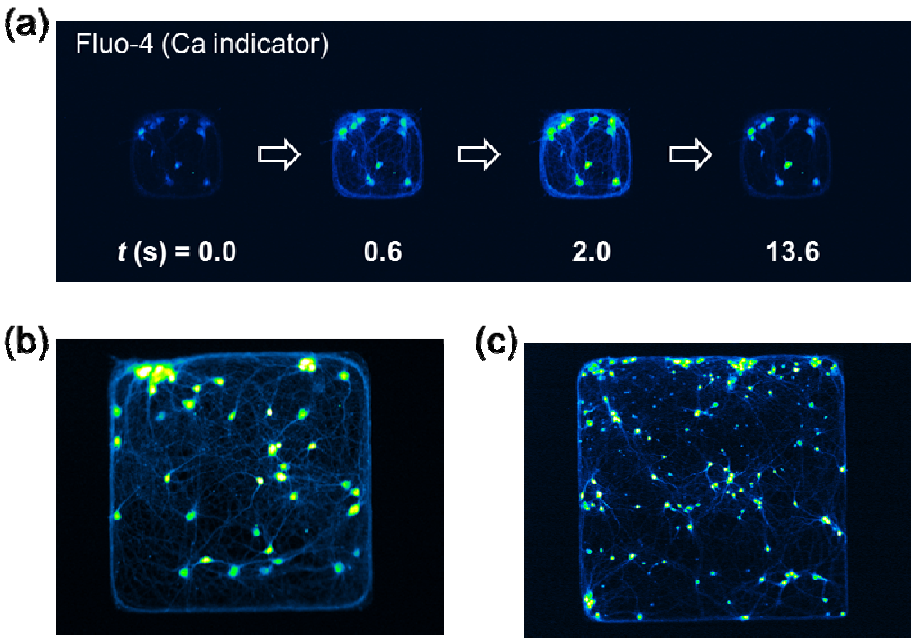

427

428 Figure 2

429

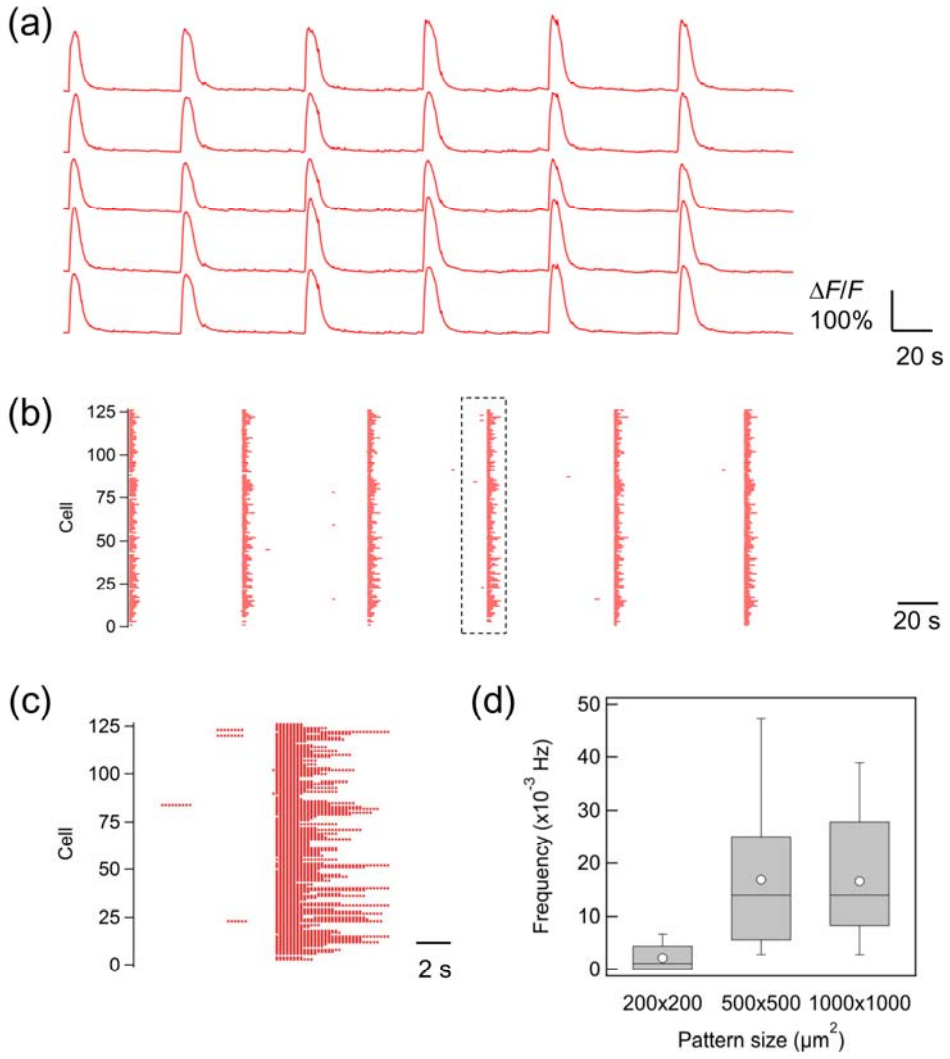
(a)
ΔF/F
100%
20 s
(b)
Cell
125
100
75
50
25
0
20 s
(c)
Cell
125
100
75
50
25
0
2 s
(d)
Frequency (x10-3 Hz)
50
40
30
20
10
0
200x200
500x500
1000x1000
Pattern size (μm2)

Figure 3

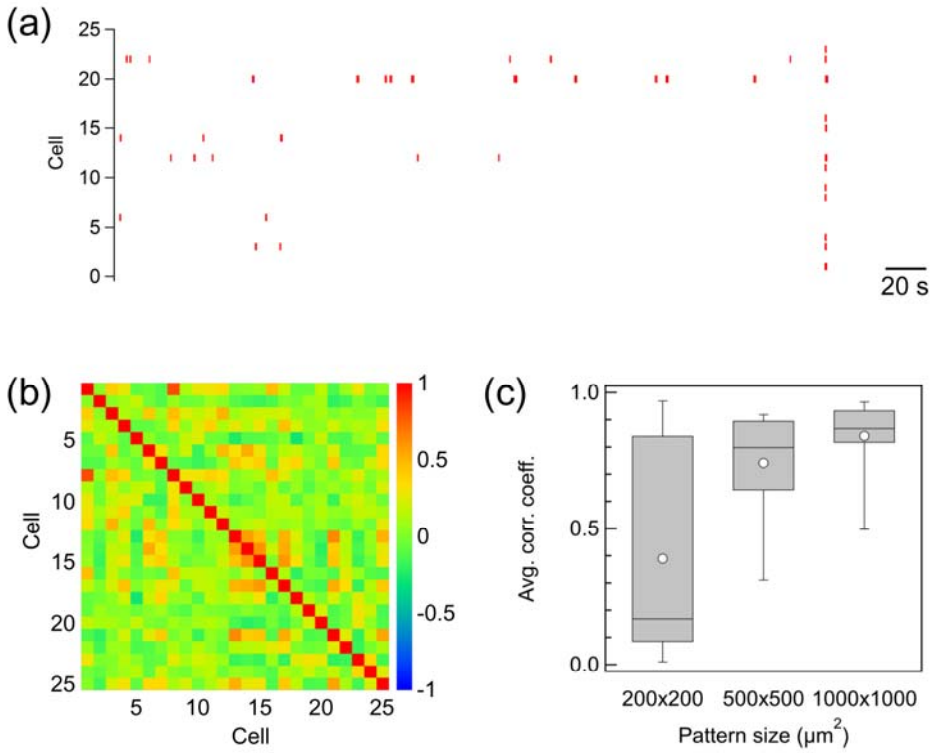
(a)
Cell
25
20
15
10
5
0
20 s
(b)
Cell
5
10
15
20
25
Cell
1
0.5
0
-0.5
-1
(c)
Avg. corr. coeff.
1.0
0.5
0.0
200x200
500x500
1000x1000
Pattern size (μm²)

Figure 4

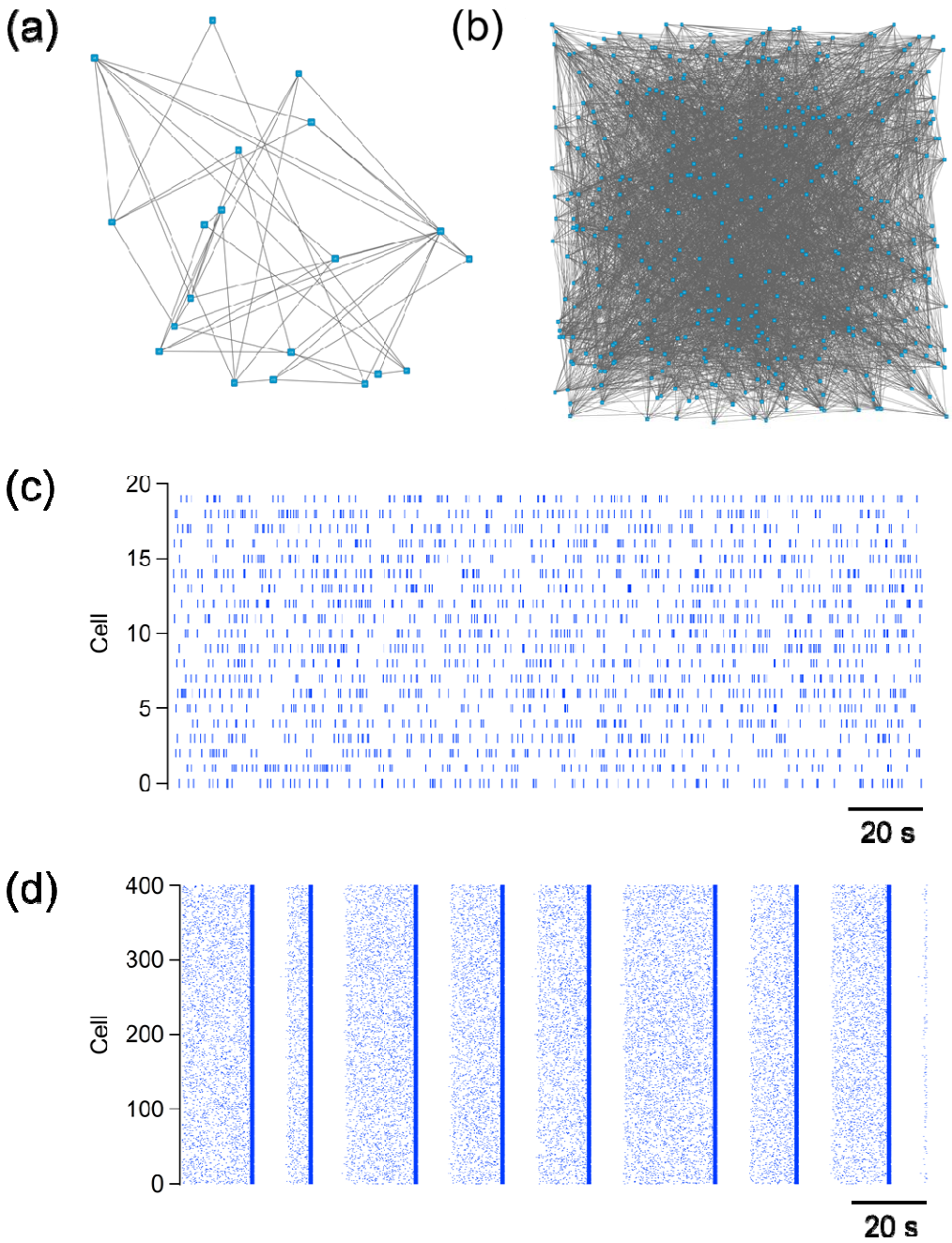

436

437 Figure 5

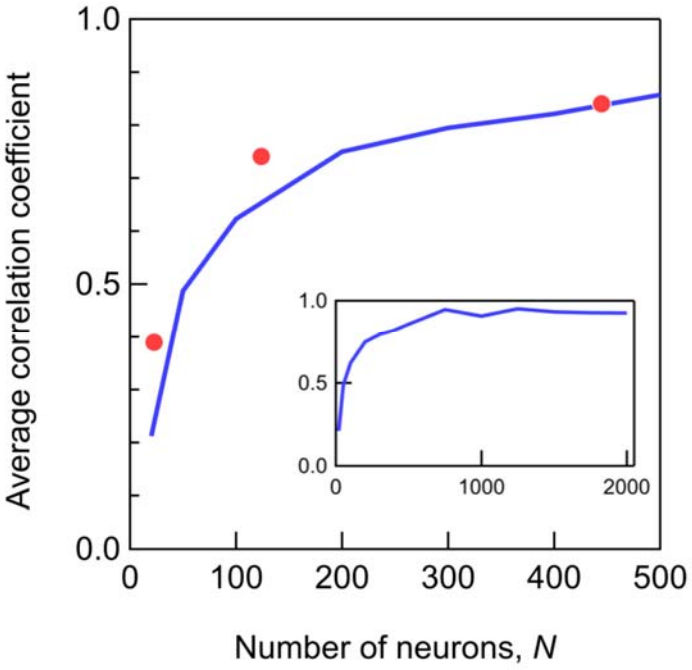

Figure 6

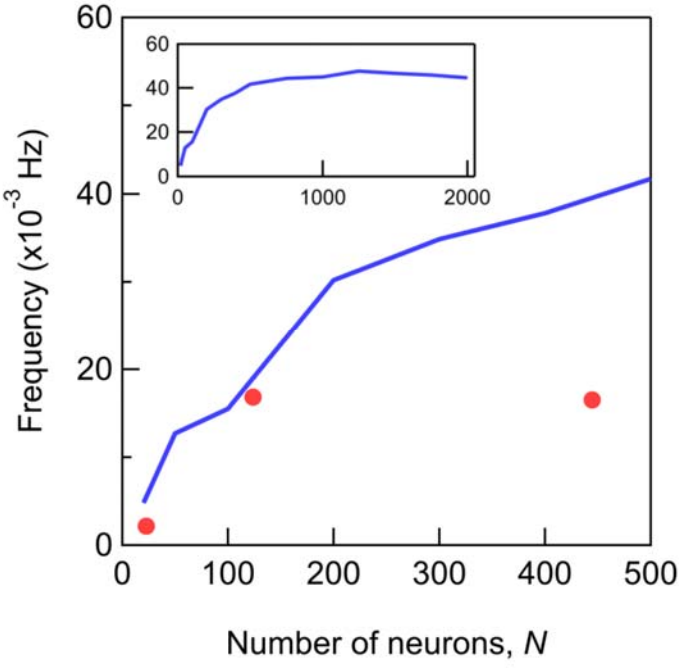

Figure 7